Investigation into geotechnical parameters of liquefied sand by static pile load tests, cone penetration tests, and pressuremeter tests

K. Toda
Chief, Construction Solutions Development Department, Giken LTD., Kochi, Japan
A. Mori
Chief, Construction Solutions Development Department, Giken LTD., Kochi, Japan
Y. Ishihara
Manager, Construction Solutions Development Department, Giken LTD., Kochi, Japan
M. Eguchi
Assistant Manager, Construction Solutions Development Department, Giken LTD., Kochi, Japan
H. H. Tamboura
Chief, Construction Solutions Development Department, Giken LTD., Kochi, Japan
S. M. K. Pasha
Construction Solutions Development Department, Giken LTD., Kochi, Japan
S. K. Haigh
Professor of Geotechnical Engineering, Department of Engineering, University of Cambridge, Cambridge, UK
A. Burakowski
Department of Engineering, University of Cambridge, Cambridge, UK

ABSTRACT

Methods using pressed-in steel sheet piles have been proposed as countermeasures against liquefaction. Research has shown the effectiveness of a square steel sheet pile wall surrounding a structure in controlling subsidence and tilting due to liquefaction, primarily by restraining the soil flow. Additionally, the structural support capabilities have been assessed through vertical and horizontal loading tests conducted on a large-scale model within the "Liquefaction Test Apparatus," which is capable of creating and maintaining a certain level of liquefaction. However, there is insufficient understanding of the ground conditions necessary for evaluating the bearing capacity of the square sheet pile wall, which is a requirement in its design process. This study aims to present fundamental test results aimed at determining the geotechnical parameters of liquefied sands in the "Liquefaction Test Apparatus." Three types of tests were conducted. The first involved static vertical and horizontal load tests conducted on square-shaped piles, equipped with strain gauges, inclinometers, and earth pressure transducers. The second test method used was Cone Penetration Testing, while the third used the Borehole Pressuremeter Test. These tests were conducted with the excess pore water pressure ratio of the model ground, specifically at ratios of 0, 0.3, 0.6, and 0.9.

Key words: *Liquefaction, Static load test, Cone Penetration Test, Borehole Pressuremeter Test*

1. Introduction

Methods using pressed-in steel sheet piles have been proposed as countermeasures against liquefaction (Ishihara et al. 2023). One such method involves square

steel sheet pile walls surrounding a structure, which effectively restrains soil flow under the structure. The efficacy of this approach in controlling subsidence and tilting due to liquefaction has been confirmed through shaking table model tests conducted under both gravitational and centrifugal fields (Kato et al. 2014). Additionally, given that steel sheet piles are used as friction piles, they are anticipated to perform well in supporting structures. The bearing capacity of either a single pressed-in tubular pile or a structure including a square steel sheet pile wall has been confirmed through a large-scale model test involving vertical and horizontal loading in the "Liquefaction Test Apparatus," under both non-liquefaction and liquefaction conditions (Willcocks 2021; Haigh 2022). This apparatus is capable of creating and maintaining a certain level of liquefaction over a specified duration by using seepage forces from the bottom to the surface of the model ground in place of seismic motion (Ogawa et al. 2018). However, the geotechnical parameters necessary for evaluating bearing capacity under liquefaction conditions have not been identified in these studies.

The purpose of this study is to present the fundamental test results aimed at determining the geotechnical parameters of liquefied sands in the "Liquefaction Test Apparatus." Three types of tests were conducted. The first one involved the static vertical and horizontal loading tests (VLT and HLT) conducted on square-shaped piles equipped with strain gauges, inclinometers, and earth pressure transducers. The second test method used the Cone Penetration Test (CPT), and the third one used the Borehole Pressuremeter Test (BPT). These tests were conducted with the excess pore water pressure ratio of the model ground, specifically at ratios of 0, 0.3, 0.6, and 0.9. Finally, as an example of the geotechnical parameters, subgrade reaction coefficients were estimated according to the Specification for Highway Bridge Part IV (JARA 2017), and their relationship to excess pore water pressure ratio was confirmed through comparison across the three tests.

2. Acquisition of excess pore water pressure ratio

As shown in **Fig. 1**, the "Liquefaction Test Apparatus" is a tank measuring 7 m x 7 m x 10 m, filled with sand, as detailed in **Table 1**. The pore pressure transducers were installed at depths of GL-1 m, GL-3 m, and GL-5 m on both the west and east sides, situated 2 m from the center. The seepage forces generated by water movement from the bottom to the top of the tank resulted in an increase in excess pore water pressure. The relationship between flow rate and excess pore water pressure, as measured by the pore pressure transducers, is shown in **Fig. 2**. The excess pore water pressure ratio (r_u) was obtained by:

$$r_u = \frac{\Delta u}{(\gamma_{sat} - \gamma_w) z} \quad (1)$$

where Δu represents the excess pore water pressure measured by the pore pressure transducers, γ_{sat} denotes the saturated unit weight as shown in **Table 1**, γ_w stands for the unit weight of the water, and z is the depth from the ground surface. As illustrated in **Fig. 3**, the difference in the excess pore water pressure ratio at each depth was small, confirming a uniform degree of liquefaction in the model ground. In the range of higher flow rates, stronger momentum was observed in the water flowing into the drainage. It was estimated that this phenomenon affected the excess pore water pressure ratios at depth GL-1 m, causing them to exceed 1.

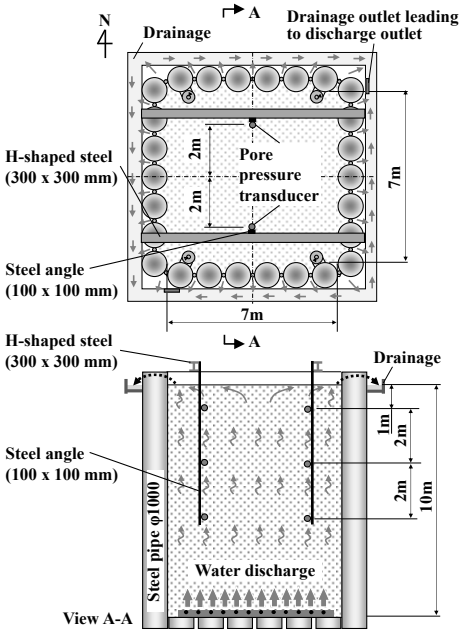

Fig. 1 Liquefaction Test Apparatus

Table 1 Sand property

Soil particle density	ρ_s	[kN/m^3]	26.3
Saturated unit weight (D_r=10%)	γ_{sat}	[kN/m^3]	18.4
Maxmum void ratio	e_{max}		0.891
Minmum void ratio	e_{min}		0.531

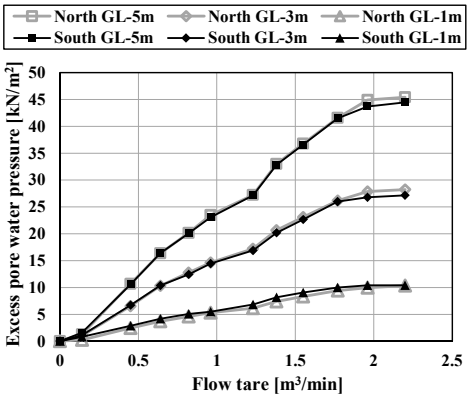

Fig. 2 Relationship between flow rate and excess pore water pressure

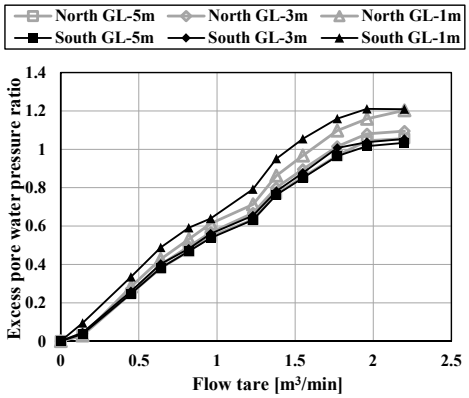

Fig. 3 Relationship between flow rate and excess pore water pressure ratio (r_u)

3. Estimation methods of the subgrade reaction coefficients

The procedure for determining the subgrade reaction coefficients from VLT, HLT, BPT, and CPT is shown in **Fig. 4**.

The subgrade reaction coefficients for VLT and HLT (k_{V_VLT} and h_{H_HLT}) were estimated from the *p-y* curves correlating soil reaction and pile deflection obtained through the respective tests. The reference displacement defining the subgrade reaction coefficients was selected to be 3 mm (1% of the 300 mm pile width) (JARA 2017).

The Young's modulus from BPT ($E_{\_BPT}$) was determined according to JGS 1421-2003 (JGS 2013). According to JARA (2017), the subgrade reaction coefficient from BPT (k_{H_BPT}) was obtained as follows:

$$k_{H\_BPT}=\lambda k_0(B'/0.3)^{-3/4} \quad [kN/m^2] \quad (2)$$

$$k_0=\alpha E_{\_BPT}/0.3 \quad [kN/m^2] \quad (3)$$

$$B'=\sqrt{D/\beta} \quad (4)$$

$$\beta=\sqrt{k_{H\_BPT}D/4EI} \quad (5)$$

where λ is the factor taking into account the construction method of the foundation (λ = 1), k_0 represents the subgrade reaction coefficient corresponding to the value from a plate loading test with a rigid disc of 0.3 m diameter, B' signifies the converted load width of the foundation, α denotes the conversion factor, α = 4 for BPT, D is the diameter of the pile, β represents the characteristic value, and EI signifies the bending stiffness of piles.

According to Robertson (2009), the Young's modulus from CPT ($E_{\_CPT}$) was determined as follows:

$$E_{\_CPT} \sim 0.8G_0=0.8\rho V_S^2 \quad [kN/m^2] \quad (6)$$

$$V_S=\left[\alpha_{vs}\left(q_t-\sigma_{V0}\right)/p_a\right]^{0.5} \quad (7)$$

$$\alpha_{vs}=\left[10^{(0.55I_c+1.68)}\right] \quad (8)$$

$$I_c=\left(\left(3.47-\log Q_t\right)^2+\left(\log F_r-1.22\right)^2\right)^{0.5} \quad (9)$$

$$Q_t=\left(q_t-\sigma_{V0}\right)/\sigma'_{V0} \quad (10)$$

$$F_r=f_s/\left(q_t-\sigma_{V0}\right)\times 100 \quad [\%] \quad (11)$$

where ρ represents mass density ($\rho = \gamma_{sat}/9.8$), V_s denotes the shear-wave velocity, α_{vs} is the shear-wave velocity factor, q_t represents the cone resistance obtained by CPT, σ_{V0} represents the total stress, p_a indicates the atmospheric pressure (P_a = 100 [kPa]), I_c represents the soil behavior type index, Q_t represents the normalized cone penetration resistance, σ'_{V0} denotes the effective stress, F_r stands for the normalized friction ratio, and f_s signifies the sleeve friction obtained by CPT. The subgrade reaction coefficient from CPT (k_{H_CPT}) was obtained by equations (2) to (5), with $E_{\_BPT}$ replaced by $E_{\_CPT}$.

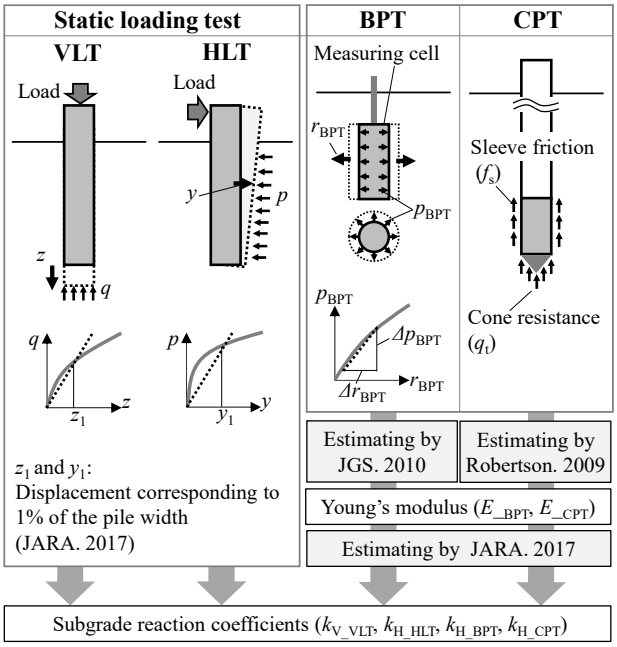

Fig. 4 Procedure for determining the subgrade reaction coefficients

4. Testing methods

4.1. Test cases

Three types of tests were conducted with r_u: 0, 0.3, 0.6, and 0.9, as shown in **Table 2**. HLT was not conducted at $r_u = 0.9$ due to observed self-settling in VLT at $r_u = 0.87$ (in V9).

Table 2 Test cases

Case	Test type		r_u (measured)
V0	Static loading test	Vertical (VLT)	0.00
V3			0.30
V6			0.60
V9			0.87
H0		Horizontal (HLT)	0.00
H3			0.23
H6			0.58
C0	Cone Penetration Test (CPT)		0.00
C3			0.33
C6			0.58
C9			0.83
B0	Borehole Pressuremeter Test (BPT)		0.00
B3			0.19
B6			0.59
B9			0.90

r_u : Excess pore water pressure ratio

4.2. Vertical and horizontal static loading tests (VLT and HLT)

As shown in **Fig. 5**, strain gauges were installed on both the west and east sides of the pile to measure axial and bending strains. Both earth pressure and pore pressure transducers were installed at depths of GL-1 m, GL-2 m, and GL-5 m below the ground surface to obtain the ground horizontal resistance acting on the test pile. Inclinometers were installed at the same depth as the aforementioned transducers.

The VLT and HLT procedures are explained below, with Steps 2, 4, and 5 illustrated in **Fig. 6**.

Step-1. Ground preparation

To eliminate the effects of the previous loading test, the model ground was subjected to complete liquefaction for 30 minutes at a flow rate of 2.0 m^3/min.

Step-2. Installing the test pile

The test pile was filled with water to prevent displacement by buoyancy forces. First, the ground was liquefied at a flow rate of 1.8 m^3/min, and the test pile was inserted under its own weight into the center of the tank to a depth of approximately 3.5 m. Subsequently, the flow rate was increased to 2.0 m^3/min, and the test pile was further inserted to a depth of 7 m.

Step-3. Curing of the ground

The test pile was allowed to cure for approximately one day. Steps 4 and 5 were carried out during curing.

Step-4. Swedish Weight Sounding (SWS) test

SWS tests were conducted 2 m west and 2 m east of the center of the test pile. The test results were presented in **Fig. 7**.

Step-5. Preparation of the test

Displacement sensors and jacks for VHL and HLT were installed as shown in **Fig. 8**. Base displacement was measured at the steel rod base, while horizontal displacement at the ground surface ($D_{H\_GL\text{-}0}$) was obtained by the displacement sensors.

Step-6. Loading test

Initially, the ground was liquefied for 10 mins at the specified excess pore water pressure ratio. Vertical or horizontal loading was then initiated while liquefaction was maintained. The loading method followed JGS 1811-2002 (JGS 2002) and JGS 1831-2010 (JGS 2010) for VLT and HLT, respectively.

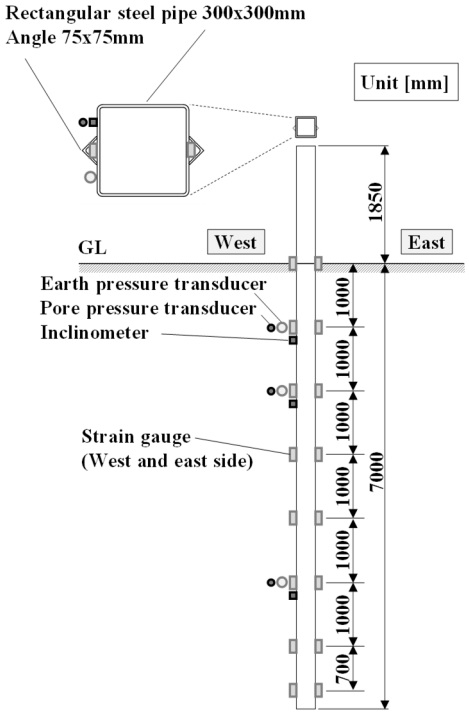

Fig. 5 Layout of the test pile

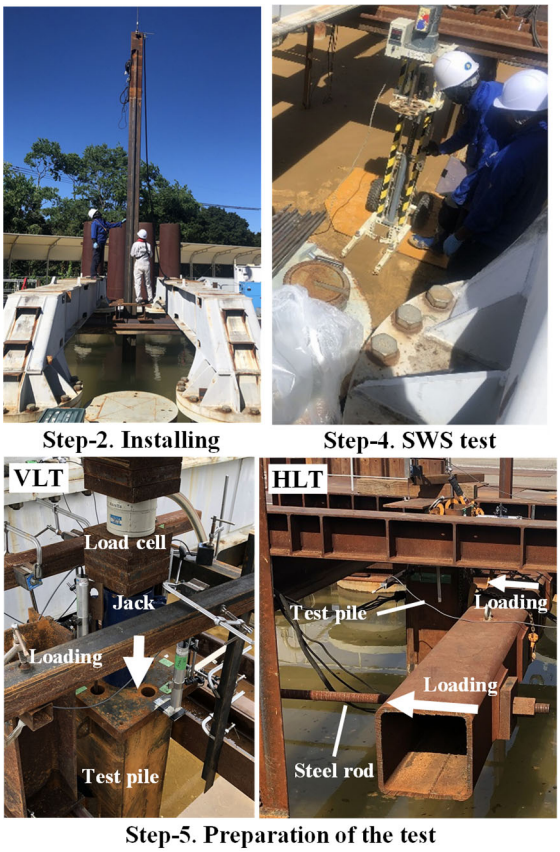

Fig. 6 Situation of pile installation, SWS test, VLT, and HLT

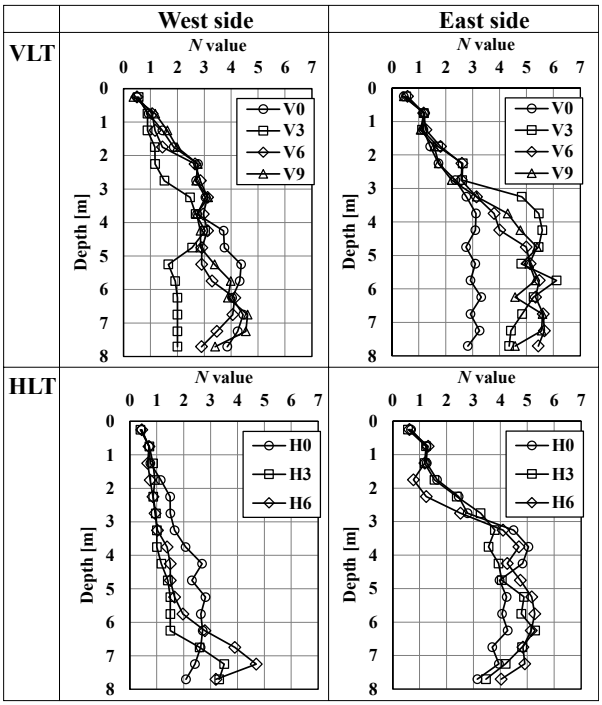

Fig. 7 SWS test results at the west and east sides

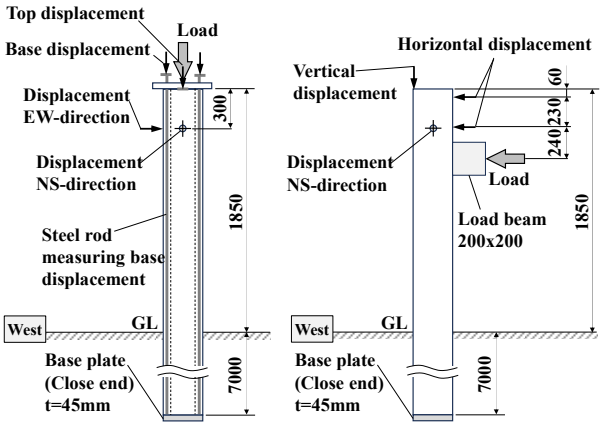

Fig. 8 Layout of VLT (left side) and HLT (right side)

4.3. Cone Penetration Test (CPT)

The CPT was conducted 2 m west of the center of the tank, as shown in **Fig. 9**. Ground preparation to eliminate the effects of previous tests was performed prior to each test.

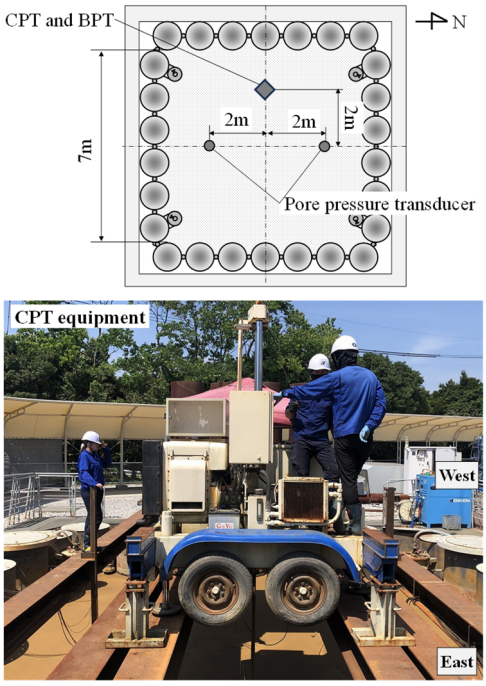

Fig. 9 Layout of CPT and BPT

4.4. Borehole Pressuremeter Test (BPT)

The BPT was positioned with the center of the probe located 2 m from the ground surface, at the same point as the CPT, as shown in **Fig. 10**. The probe was inserted by liquefying the ground, so there was no excavation hole and the probe was in contact with the ground. Ground preparation to eliminate the effects of previous tests was also performed prior to each test.

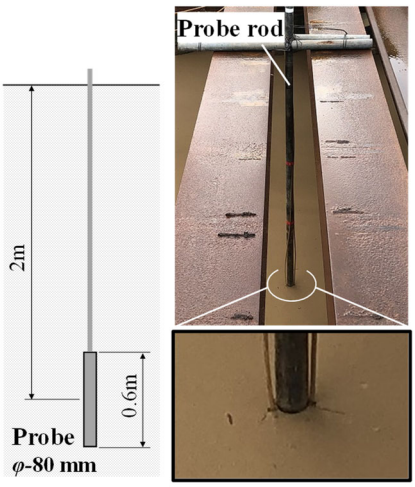

Fig. 10 BPT before tests

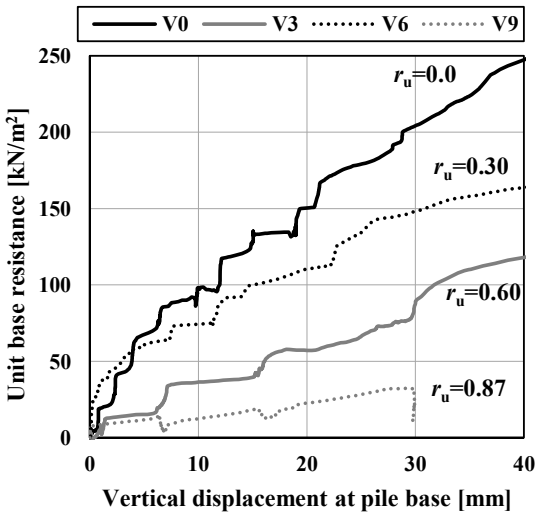

Fig. 12 *p-y* curves obtained by VLT at pile base

5. Test results

5.1. Vertical and horizontal static loading test (VLT and HLT) results

The vertical load-displacement curves and the *q-z* curves of base resistance in all cases were obtained, as shown in **Figs. 11** and **12**. Unit base resistance was calculated using strain gauges positioned 0.3 m above the pile base. However, in the case of V9, stable values for strain at 0.3 m above the pile base could not be obtained, so values at 1.0 m above the pile base were used. The stiffness at the pile head and base was observed to decrease as r_u increased.

Horizontal load-displacement curves were obtained, as shown in **Fig. 13**. The stiffness was observed to decrease, similar to VLT.

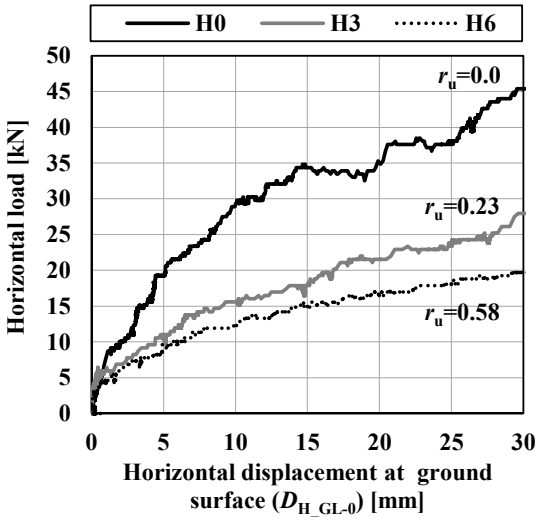

Fig. 13 Horizontal load-displacement curve

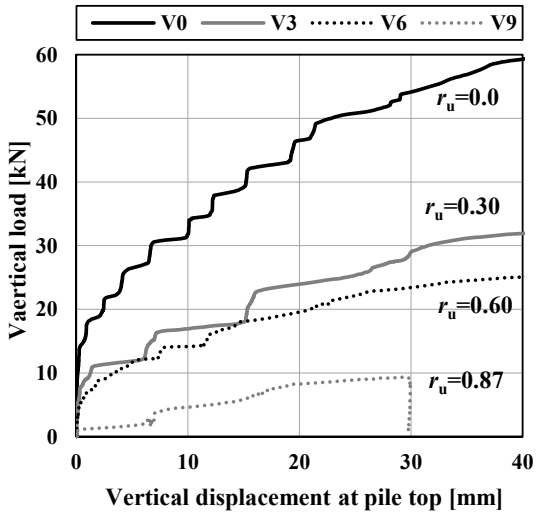

Fig. 11 Vertical load-displacement curve

The horizontal displacement required to obtain the *p-y* curves of horizontal resistance was estimated using strain gauges installed on the test pile, based on the following procedure:

Firstly, the bending moment was obtained using the strain gauges, and this distribution was calculated using a polynomial approximation curve of the seventh order. The bending moment at the loading point and the test pile base was assumed to be zero. The bending moment distributions were obtained for D_{H_GL-0} of 15 mm, as shown in **Fig. 14** of the left side.

Secondly, the rotation angle was calculated by integrating the bending moments mentioned above, with the initial value at the pile tip assumed to be zero. Cases V3 and V6 were adjusted to match the value of the

inclinometer at GL-2 m as the rotation of the pile tip was inferred. As shown in **Fig. 14** on the right side, the calculated values correspond to the measurements. However, the rotation angle at GL-5 m was not obtained due to the sensor failure in cases H3 and H6.

Finally, the horizontal displacement was calculated by integrating the rotation angles obtained above, with the displacement of the load point being the value obtained from the displacement sensors, as shown in **Fig. 15**.

The *p-y* curves of horizontal resistance at GL-2 m were obtained, as shown in **Fig. 16.** The horizontal earth pressure was measured using the earth pressure transducer installed on the test pile. It was observed that stiffness decreased as r_u increased.

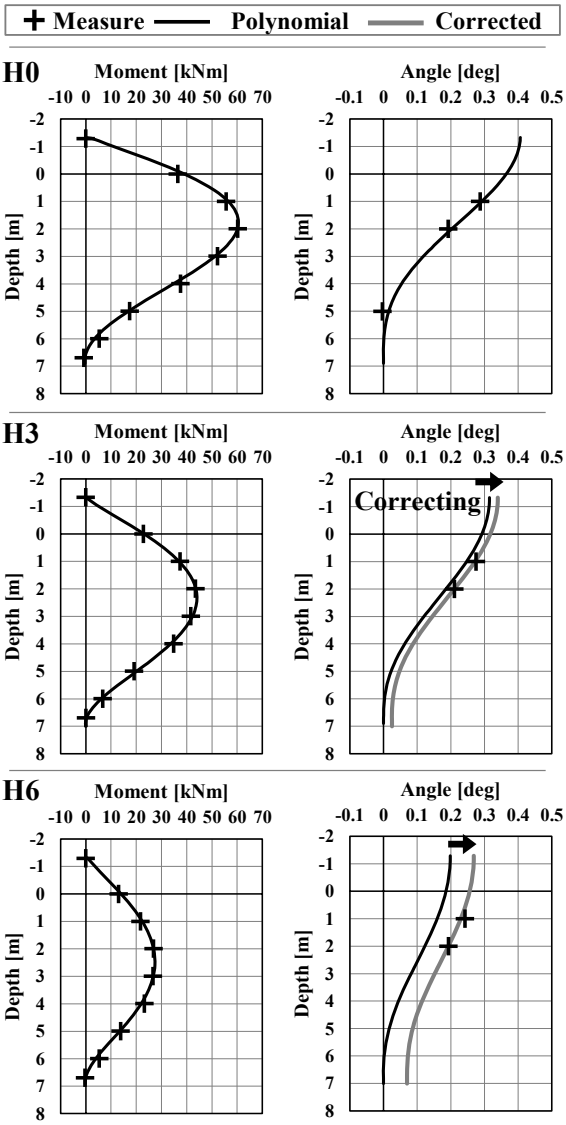

Fig. 14 Distribution of bending moment and rotation angle when $D_{H\_GL\text{-}0}$ was 15 mm

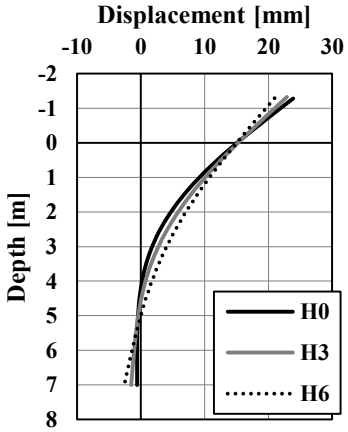

Fig. 15 Distribution of horizontal displacement when $D_{H\_GL\text{-}0}$ was 15 mm

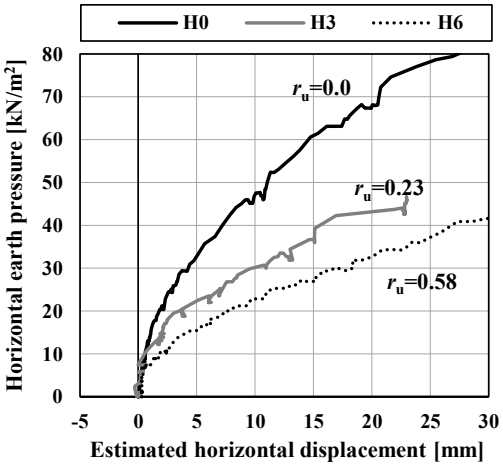

Fig. 16 *p-y* curves obtained by HLT at GL-2 m

5.2. Cone Penetration Test (CPT) results

Results of q_t, f_s, and pore water pressure (u) were obtained, as shown in **Fig. 17**. It was observed that cone resistance decreased as r_u increased, and the ratio of C0 to C9 generally ranged approximately 35% in the depth direction and was larger than at the base, which was 15%. The rate of decrease in f_s was small from case C0 to case C6 but significant at case C9. One reason for this different trend may be attributed to the dynamic effect of the penetration speed (2 cm/sec). Accurate values of u could not be obtained up to 1 m above the surface due to the instability of the rod angle. In all cases, u increased proportionally with depth. The excess pore water pressure generated by the "Liquefaction Test Apparatus" was generally considered to be evenly distributed in the depth direction, as discussed in Chapter 2.

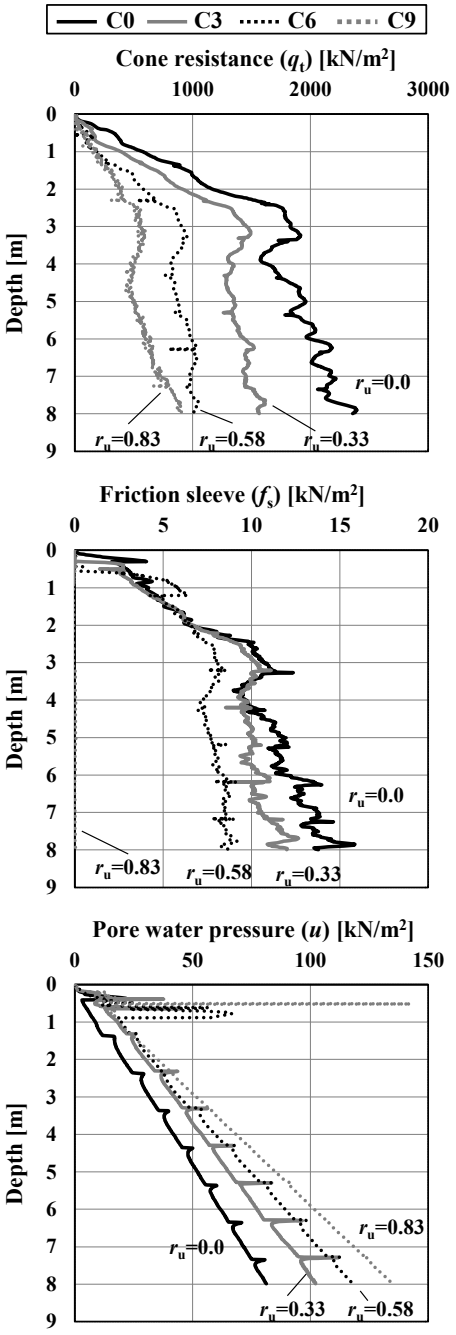

Fig. 17 Results of cone resistance (q_t), friction sleeve (f_s), and pore water pressure (u)

5.3. Borehole Pressuremeter Test (BPT) results

The p_{BPT}-Δr_{BPT} curves of the BPT were obtained, as shown in **Fig. 18**. The initial stiffness below 2 mm did not significantly differ across all cases. Subsequently, with the exception of case P3, the probe pressure decreased as r_u increased. Although the ground preparation reset the effects of the previous test, case P3 may have had stiffer ground before liquefaction compared to other cases.

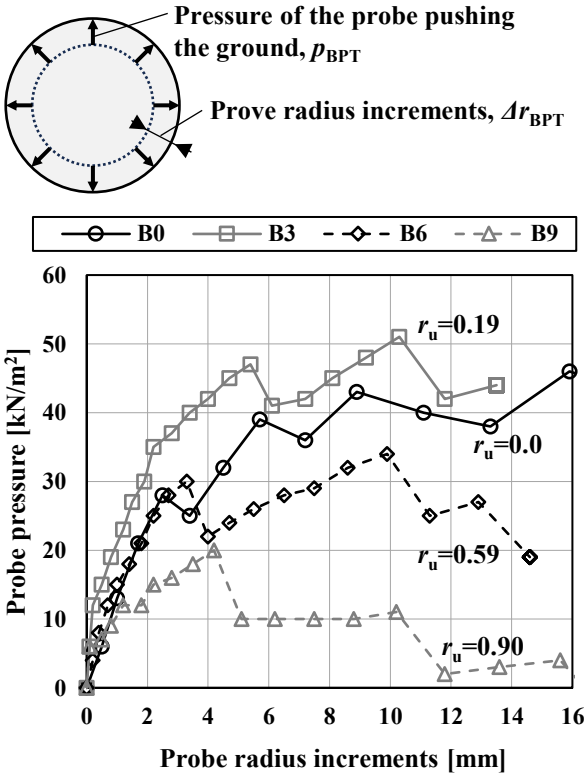

Fig. 18 Horizontal resistance stiffness for BPT

6. Subgrade reaction coefficients (k)

The subgrade reaction coefficients for the three tests were estimated using the methods outlined in Chapter 3.

For static loading tests of VLT and HLT, k_{V_VLT} and k_{H_HLT} were obtained, as shown in **Fig. 19**. With the exception of case V6, a linear trend of decreasing subgrade reaction coefficients was confirmed. The averaged N values of V0, V3, V6, and V9 from GL-7 m to GL-7.3 m east and west, shown in **Fig. 7,** were 4.0, 3.2, 4.8, and 5.1, respectively, with V6 being higher than V0 and V3. One possible factor contributing to the exceptional trend of V6 is considered to be the variation of N values.

Regarding the estimation derived from the CPT results, the variation of k_{H_CPT} with depth is shown in **Fig. 20 (a)**, while the relationship between k_{H_CPT} and r_u at a depth of 2 m is illustrated in **Fig. 20 (b)**. For C9, the f_s was zero, rendering estimation unattainable beyond GL-3 m. The relationship between k_{H_CPT} and r_u was confirmed to exhibit linear agreement.

In the context of the BPT, the coefficient k_{H_BPT} was derived from the linear section of the p_{BPT}-Δr_{BPT} curve. The relationship between k_{H_BPT} and r_u is shown in **Fig. 21**, where the observed trend was confirmed.

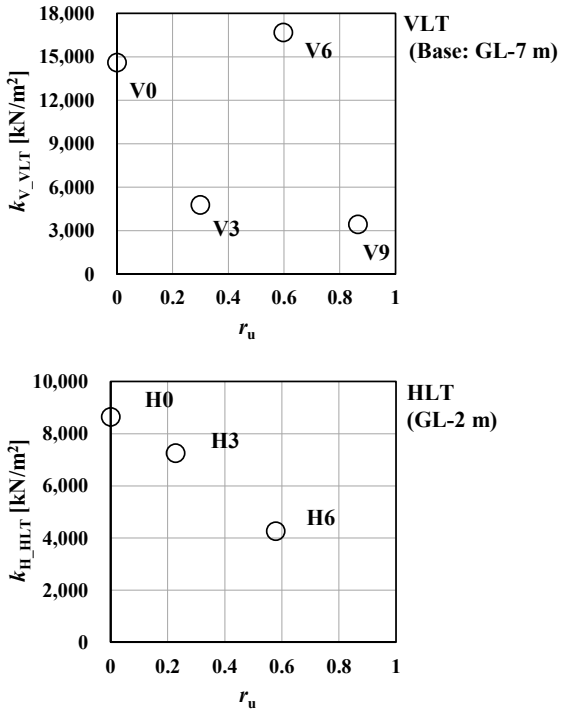

Fig. 19 Relationship between k_{V_VLT} or k_{H_HLT} and r_u

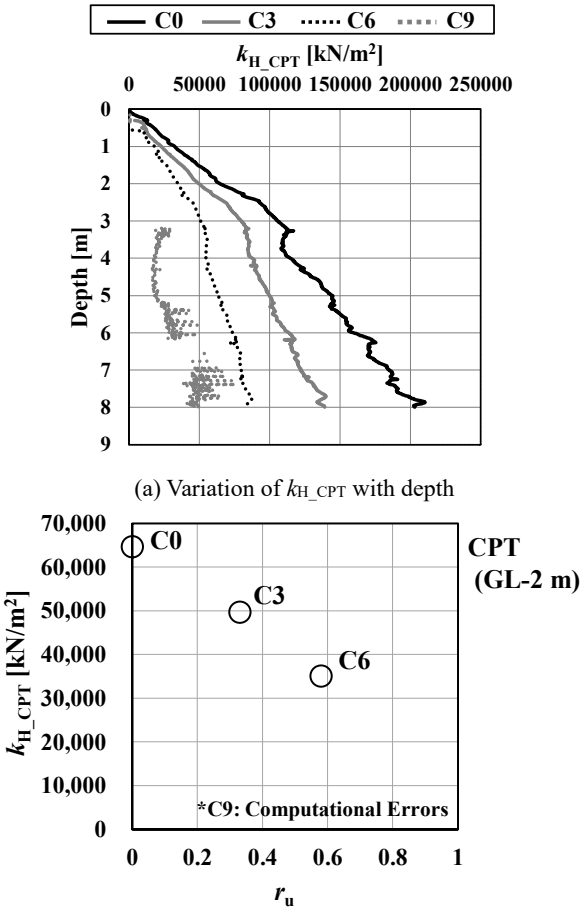

(a) Variation of k_{H_CPT} with depth

(b) Relationship between k_{H_CPT} and r_u

Fig. 20 k_{H_CPT} estimated from the CPT results

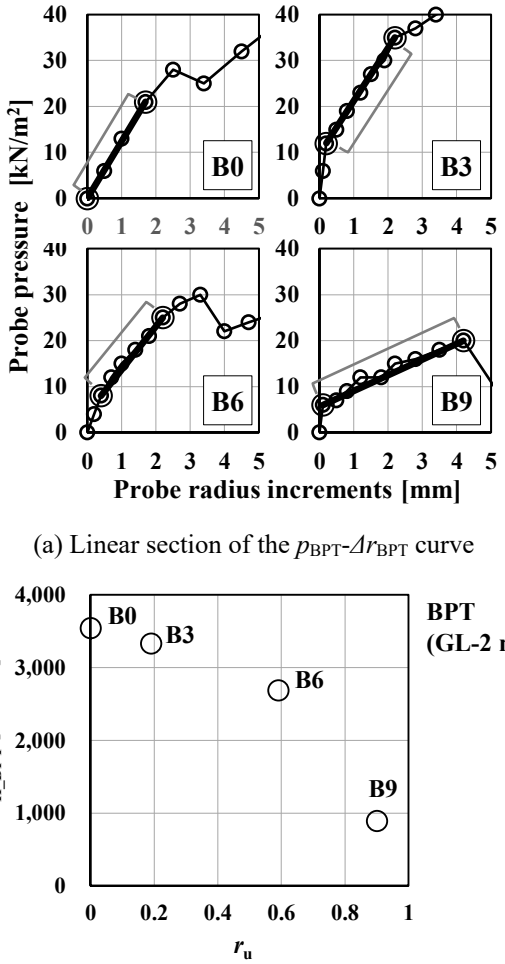

(a) Linear section of the p_{BPT}-Δr_{BPT} curve

(b) Relationship between k_{H_BPT} and r_u

Fig. 21 k_{H_BPT} estimated from the BPT results

The subgrade reaction coefficients, normalized at r_u = 0, were obtained, as shown in **Table 3**. At GL-2 m, the subgrade reaction coefficients derived from CPT data were approximately ten times higher than those from BPT. This discrepancy is attributed to an oversight of strain level differences not taken into account. For instance, it has been confirmed that Young's modulus obtained from shear-wave velocity is 10–40 times higher than that obtained from BPT (Anai et al. 2018). The subgrade reaction coefficients, as indicated by the results of this study, showed similar differences. When addressing ground parameters during liquefaction, it is important to consider differences in strain levels.

The relationship between the subgrade reaction coefficients normalized at r_u = 0 and r_u is shown in **Fig. 22**. While a different decreasing trend for VLT was previously confirmed, the decreasing trend for HLT, CPT, and BPT was confirmed to be similar.

Table 3 Subgrade reaction coefficients (k) normalized at $r_u = 0$

Test (Depth)	Case	r_u	k [kN/m^2]	Normalized at $r_u = 0$
VLT (GL-7 m)	V0	0.00	14,628	1.00
	V3	0.30	4,784	0.33
	V6	0.60	16,691	1.14
	V9	0.87	3,442	0.24
HLT (GL-2 m)	H0	0.00	8,650	1.00
	H3	0.23	7,261	0.84
	H6	0.58	4,276	0.49
CPT (GL-2 m)	C0	0.00	64,652	1.00
	C3	0.33	49,680	0.77
	C6	0.58	35,088	0.54
	C9	0.83	-	-
BPT (GL-2 m)	B0	0.00	3,546	1.00
	B3	0.19	3,333	0.94
	B6	0.59	2,689	0.76
	B9	0.90	895	0.25

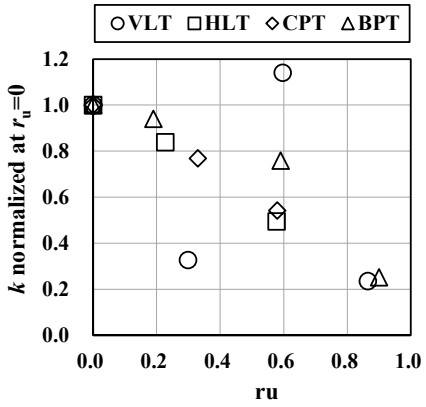

Fig. 22 Relationship between subgrade reaction coefficients (k) normalized at ru = 0 and r_u

7. Conclusions

The vertical load test, horizontal load test, CPT, and Borehole Pressuremeter Tests were conducted under varying excess pore water pressure ratios of the ground at 0, 0.3, 0.6, and 0.9 using the "Liquefaction Test Apparatus."

The subgrade reaction coefficients were determined through the examination of (1) the q-z or p-y curves representing base and horizontal resistance in the static loading test, (2) analysis of the CPT cone resistance and friction sleeve, and (3) assessment of the p_{BPT}-Δr_{BPT} curves derived from the Borehole Pressuremeter test.

These subgrade reaction coefficients showed a tendency to decrease with an increase in the excess pore water pressure ratio, although the values were observed to vary depending on the testing method. This variability may be attributed to the lack of consideration for differences in strain levels.

Acknowledgements

The Borehole Pressuremeter Tests were conducted by Nishimura, H. from Soai Co., Ltd.

References

Anai, K., Yoshida, M., Mtsutoki, K. 2018. Relationship between PS logging test result and horizontal borehole loading test result about modulus of deformation. Congress of the Architectural Institute of Japan, Summaries of technical papers of annual meeting (Tohoku), September 2018.

Haigh, A. 2022. Performance of implant structures. M.Eng. Thesis, University of Cambridge, 52p.

Ishihara, Y., Ogawa, N., Eguchi, M., Toda, K. et al. 2023. R & D activities on the structures constructed by the press-in method. IPA Newsletter, Volume 8, Issue 3, September 2023, pp.9-14.

Japanese Geotechnical Society (JGS). 2002. Method for static axial compressive load test of single piles, pp.49-53.

Japanese Geotechnical Society (JGS). 2010. Method for lateral load test of piles, pp.35-40.

Japanese Geotechnical Society (JGS). 2013. Japanese standards for geotechnical and geoenvironmental investigation methos - Standards and explanations –, pp.319-327.

Japan Road Association (JARA). 2017. Specifications for highway bridges, Part IV Substructures, 586p.

Kato, I., Hamada, M., Higuchi, S., Kimura, H. and Kimura, Y. 2014. Effectiveness of the sheet pile wall against house subsidence and tilting induced by liquefaction. Journal of Japan Association for Earthquake Engineering, 14(4), pp. 4_35-4_49.

Ogawa., N., Ishihara, Y., Ono, K., Hamada, M. 2018. A large scale model experiment on the effect of sheet pile wall on reducing the damage of oil tank due to liquefaction. Proceedings of the First International Conference on Press-in Engineering 2018, Kochi.

Robertson, P. K. 2009. Interpretation of cone penetration tests – a unified approach. Canadian Geotechnical Journal, 46, pp.1337-1355.

Willcocks, F. 2021. The vertical and horizontal performance of pressed-in tubular piles in liquefied ground. M.Eng. Thesis, University of Cambridge, 47p.